Charge and mass distributions in strongly damped reactions of ^{58}Ni + ^{165}Ho at 16 MeV/nucleon

V. Penumetcha and G. A. Petitt
Department of Physics and Astronomy, Georgia State University, Atlanta, Georgia 30303

T. C. Awes, J. R. Beene, R. L. Ferguson, F. E. Obenshain, F. Plasil, and G. R. Young
Oak Ridge National Laboratory, Oak Ridge, Tennessee 37831

S. P. Sorensen
Department of Physics and Astronomy, University of Tennessee, Knoxville, Tennessee 37996 and Oak Ridge National Laboratory, Oak Ridge, Tennessee 37831

(Received 16 March 1990)

Secondary charge and mass distributions have been measured for projectilelike fragments (PLF's) in strongly damped reactions of ^{58}Ni + ^{165}Ho at 16 MeV per nucleon bombarding energy. Statistical model evaporation calculations were compared with these distributions and with neutron multiplicities and temperatures for PLF and targetlike fragments (TLF's) to obtain the primary distributions prior to light-particle emission. The deduced primary distributions indicate a net transfer of protons to the target in contrast to the predictions of the nucleon transport exchange model, which predicts a net transfer of neutrons to the projectile. The results suggest an equal division of the available excitation energy at small total kinetic-energy (TKE) losses (up to 200 MeV) with thermal energy division occurring only at the largest TKE losses (≈325 MeV).

I. INTRODUCTION

General features of strongly damped reactions between heavy nuclei at bombarding energies near or slightly above the Coulomb barrier have been successfully described by dynamical transport models.[1-4] Knowledge of the primary reaction products following scission of the dinuclear complex is required to test these models rigorously. In order to make comparisons with the models, it is necessary to reconstruct the primary distributions of charge, mass, and excitation energy from measurements of secondary distributions and light particle emission spectra. To obtain the primary distributions from measured post-evaporative data, significant corrections must be applied to account for deexcitation of the highly excited primary products.[5] These corrections require application of reliable statistical evaporation models and a knowledge of how the available excitation energy is divided between the reaction products at scission of the dinuclear complex.

The question of this energy division is a subject of much current interest.[6-27] Several early experiments concluded that the excitation energy was divided between the primary fragments in proportion to their mass, indicating that complete statistical equilibrium was obtained between the fragments during the collision.[6-12] Recently, however, reports of several experiments have indicated that the available excitation energy is divided equally between the primary fragments, at least for small total kinetic-energy (TKE) losses.[15-26] Further measurements at larger bombarding energies can provide additional information on the evolution of the energy division process due to the expanded range of TKE losses as compared to the measurements reported so far.

Two recent comparisons[23,24] with the nucleon exchange transport model[3] of the evolution of heavy-fragment charge distributions as a function of TKE loss reach conclusions which are somewhat contradictory to each other. One study[23] of the reaction ^{74}Ge+^{165}Ho at 8.5 MeV/nucleon, which involved the measurement of the mass, charge, and angle of the PLF together with the angle of the coincident TLF, concluded that the measured centroids of the fragment nuclide distributions evolve in the opposite direction with increasing TKE loss from the direction predicted by the nucleon exchange model. In contrast, another recent study of neutron emission from products of the reaction ^{40}Ar+^{139}La at 15 MeV/nucleon reports overall agreement with the predictions of the nucleon-exchange model.[24] These experiments are typical of those made over the last few years to test the nucleon exchange model in that they involve either measurements of the multiplicities and spectral shapes for neutron emission from the reaction partners or measurements of charge and mass distributions of the PLF's. In order to obtain a reliable reconstruction of the primary distribution it is necessary to have sufficient experimental observables to overconstrain the calculated effects of evaporation. Therefore, in the experiments reported here we have measured post-evaporative charges and masses of PLF's, and multiplicities and energies of neutrons emit-

ted from PLF's and TLF's. We have compared these results with the predictions of statistical model evaporation calculations to determine the primary charge and mass distributions and the division of available excitation energy between the primary reaction fragments.

The system studied was ^{58}Ni+^{165}Ho at 16 MeV/nucleon. Because of the approximate 3:1 mass ratio of target to projectile the excitation of the PLF will be quite different, depending on whether the available excitation energy is shared equally or according to the mass ratio of the reaction fragments. The target ^{165}Ho does not fission easily, reducing the number of events with three heavy fragments in the exit channel.

II. EXPERIMENT

The experiment was performed in two parts at the Holifield Heavy Ion Research Facility (HHIRF) of the Oak Ridge National Laboratory using coupled operation of the electrostatic accelerator and cyclotron. In the first part of the experiment neutron multiplicities and temperatures of PLF and TLF were obtained from moving source fits to neutron energy spectra. These results are described in detail elsewhere.[28] Secondary charges and masses of PLF's were measured in the second part of the experiment. The heavy-ion time-of-flight facility at the HHIRF was used for these measurements. This apparatus consists of a scattering chamber connected to a large area ionization chamber by a flight path of 2.4 m length. Figure 1 gives a schematic view of the experimental setup. A 910-MeV pulsed beam of ^{58}Ni ions was used to bombard a ^{165}Ho metal target of 2.02 mg/cm^2 thickness. A 10 kV potential was applied to the target to suppress emission of electrons. Post evaporative charge, mass, and energy of PLF's were measured by a large-area ΔE-ΔE-ΔE-E ionization chamber located at the end of the flight arm. The ionization chamber was operated with CF_4 gas at a pressure of 155 Torr which was sufficient to stop the elastically scattered ^{58}Ni in the E element. The relative calibration of each element of the ionization chamber was obtained by injecting the same charge into the input of the electronics of each section. The absolute energy calibration was obtained from the elastically scattered beam. A position-sensitive multiwire proportional counter was placed just before the ionization chamber to account for the position dependence of energy signals from this detector. This proportional counter was operated with isobutane gas at a pressure of 3.1 Torr. A small position dependence (2%) was observed for energy signals in the direction of charge drift which was attributed to the recombination of charges before they are collected by the electrode plates. This dependence was corrected event by event offline. The observed PLF energies have been corrected for energy losses in half of the target thickness, microchannel plates, proportional counter and the entrance window of the ionization chamber. This procedure yielded an energy resolution (FWHM) of 1.2% and an overall charge resolution of less than 0.5 charge units.

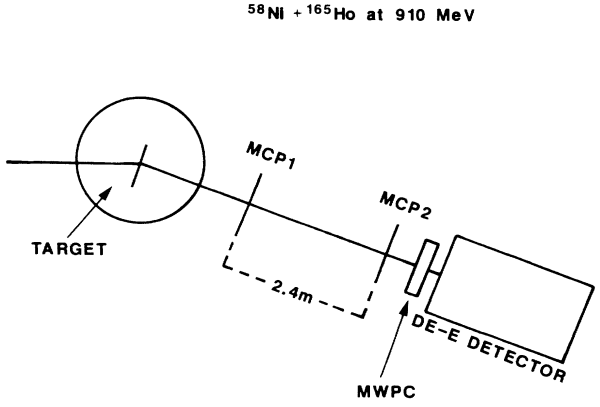

FIG. 1. Schematic diagram of the experimental setup.

The PLF time-of-flight information, to measure mass, was obtained with two microchannel plate fast-timing detectors separated by a flight path of 2.4 m. The first microchannel plate was placed at a distance of 44 cm from the target. A 28 mm diameter aperture was used before the first channel plate which limited the angular acceptance of the flight path arm to 0.15 msr. Post-evaporative mass (A) was then deduced event by event, using the relation

$$A = 2E(T_{\mathrm{TOF}} + T_0)^2/D^2 \quad (1)$$

where E is the energy of the PLF after the first microchannel plate, T_{TOF} is the measured time of flight, T_0 is the time-of-flight offset due to electronic propagation delay differences and different cable lengths, and D is the distance between the microchannel plates. The TKE loss was deduced from the measured values of E, Z, and A assuming two-body kinematics. During the experiment the time-of-flight arm was positioned at three different angles (5°, 10°, and 15°). Systematic errors in the quoted first and second moments of the measured charge and mass distributions are estimated to be less than 5% for TKE losses up to 300 MeV and less than 10% for higher energy losses. These errors arise mainly due to the increasing inefficiency of the time-of-flight system for decreasing ion mass. Statistical errors were smaller than the data points.

The distributions of secondary charges and masses of PLF's measured at a laboratory angle of 10° are shown as a function of total energy in Fig. 2. The elastic peak for both charge and mass distributions is quite visible as well as the excellent charge and mass resolution. The values of charge and mass for subsequent ridges are assigned with respect to the elastic ridge. In this way charges down to Z=5 and masses down to A=20 were identified. The angle integrated total distributions are then divided into TKE loss bins of 25 MeV width and the first (centroid) and second (variance) moments were obtained by moment analysis. The results of this analysis are tabulated in Table I and shown in Fig. 3. A strong drift with

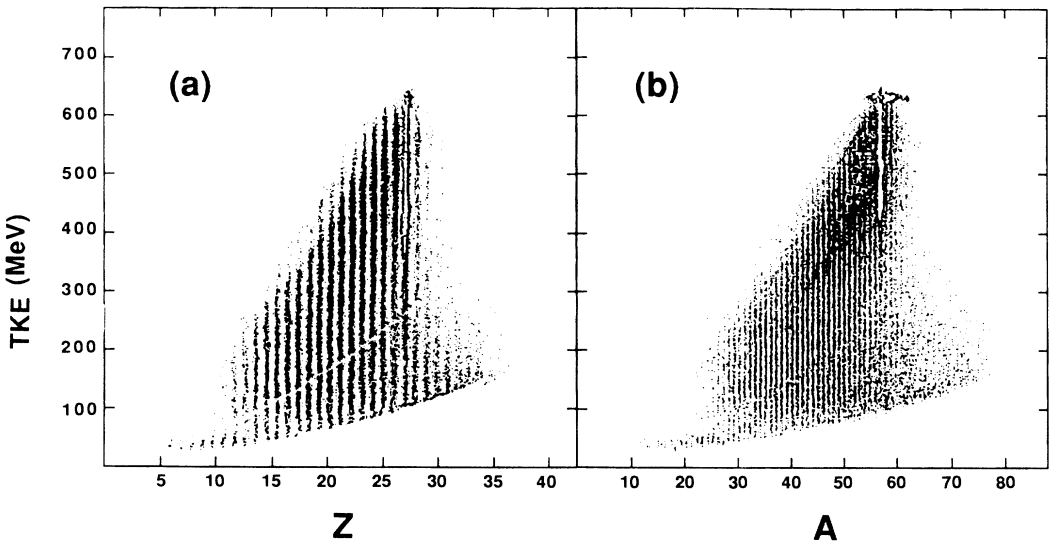

FIG. 2. Scatter plot of secondary PLF (a) charge and (b) mass versus total kinetic energy for the ^{58}Ni + ^{165}Ho reaction at 910 MeV incident energy.

increasing energy loss of the charge and mass centroids towards charges and masses smaller than that of the projectile is evident up to an energy loss of 400 MeV. The drifts to higher values above 400 MeV may be due to fusion fission but may also be due to the limitations of the detection apparatus. Because of this, further analysis of the data was confined to energy losses of less than 400 MeV.

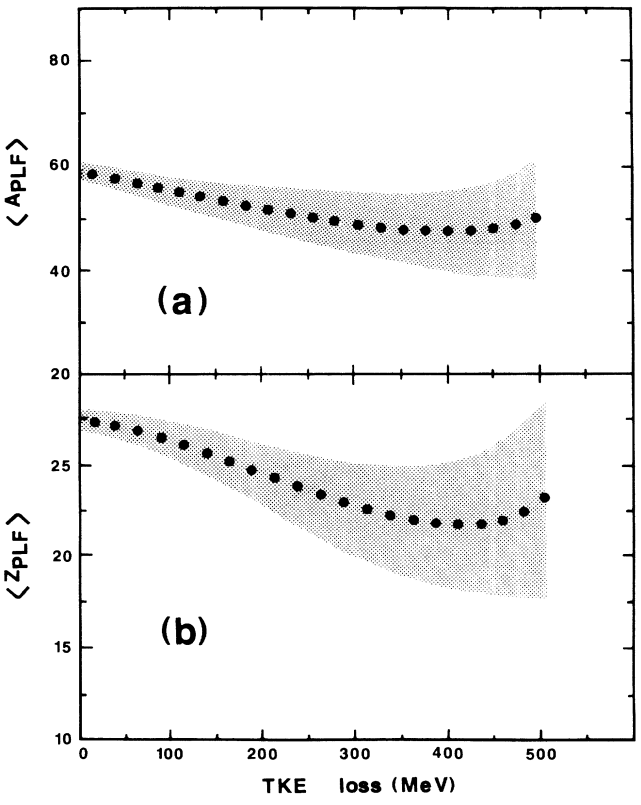

FIG. 3. Centroids of secondary PLF distributions in (a) charge and (b) mass as a function of TKE loss, determined from a moment analysis. The shaded areas surrounding the data points extend to one standard deviation from the average values.

III. ANALYSIS

We have performed evaporation calculations to extract the primary distributions using a modified version of the evaporation code LILITA.[29] A primary distribution at a given excitation energy is used as input to the code. This primary distribution is sampled by a bivariate distribution in proton and neutron number and Gaussian distributions in dissipated angular momentum and in the rel-

TABLE I. Results of a moment analysis of measured PLF charge and mass integrated over angles 5°, 10°, and 15°. The first (centroid) and second (variance) moments of the charge and mass distributions are shown as a function of TKE loss.

TKE loss (MeV)	$\langle Z \rangle$	$\langle A \rangle$	σ_Z^2	σ_A^2
12.5	28.0	58.2	0.05	0.41
37.5	27.4	57.4	0.53	1.55
62.5	27.1	56.9	0.89	2.78
87.5	26.8	56.4	1.38	4.04
112.5	26.0	54.9	1.51	4.61
137.5	25.6	54.2	2.00	6.55
162.5	25.2	53.4	2.15	7.32
187.5	24.7	52.6	2.61	9.67
212.5	24.4	51.9	3.01	11.69
237.5	24.0	51.3	3.61	14.69
262.5	23.6	50.5	3.84	17.24
287.5	23.2	49.6	4.68	21.09
312.5	22.8	48.7	5.00	23.12
337.5	22.3	47.8	6.70	31.24
362.5	22.1	47.4	8.25	39.82
387.5	21.8	46.9	10.02	48.02
412.5	21.7	46.6	12.42	60.31
437.5	21.6	46.5	15.73	76.38

ative sharing of excitation energy between the two-body reaction partners. The decay of the reaction products is calculated using the Hauser-Feshbach formula in conjunction with the Monte Carlo method. The history of the excited nucleus is followed until insufficient excitation energy remains for further decay by light particles or when an angular momentum in the entrance channel is reached for which there is no possible coupling to the exit channel angular momentum. The code uses a constant-temperature approximation to the Fermi-gas level density in the continuum region. The procedure used to calculate the TKE loss in this evaporation code is the same as the procedure used in the data analysis to calculate the TKE loss event by event.[28] This enabled us to compare the statistical evaporation code predictions directly with the data. The predictions of this statistical evaporation code have been compared to those of PACE[30] for representative cases and found to produce similar results.

For the calculations presented here the dissipated angular momentum (l) was assumed to increase linearly from zero at no energy loss to the sticking limit at the Coulomb barrier. The variance in angular momentum used for the simulation is given by $\sigma_l = 0.3\langle l \rangle$. This choice of σ_l is a conservative estimate of the fluctuations in the transferred angular momentum.[31] Depending on the choice of model, they could be larger, but we have chosen to use the most conservative estimate. As described below, the primary mass and charge distribution and the relative sharing of the available excitation energy used as input to the evaporation code were varied until the observed PLF secondary charge and mass centroids, and PLF and TLF neutron multiplicities and temperatures (logarithmic slope parameters of neutron energy spectra) were reproduced. Temperatures, which are not directly calculated by the evaporation code, were obtained in the following way: Angle-integrated neutron energy spectra were constructed from the evaporated neutrons generated in the evaporation code for PLF and TLF separately. These PLF and TLF spectra were then fitted using the function

$$N(E) = A\sqrt{E}\exp(-E/T)\,, \tag{2}$$

where E is the neutron energy and T is the temperature. In this way temperatures were obtained in a fashion analogous to those obtained in Ref. 28. (In order to avoid confusion in the following discussion, we will refer to temperatures resulting from fits to the Monte Carlo–generated spectra as "calculated" values and the temperatures obtained from moving source fits to the actual neutron spectra as "observed" values.) In this analysis, the division of excitation energy between the reaction fragments was not assumed *a priori* but treated as a free parameter. The calculated secondary charge and mass centroids, temperatures, and neutron multiplicities were found to be quite insensitive to extreme variations (doubling the values) of the primary variances σ_Z^2, and σ_N^2.

IV. RESULTS

We first illustrate the effects of using very different divisions of excitation energy between the reaction partners with the primary charge and mass centroids fixed at the entrance channel values. The results of these calculations are shown in Figs. 4–6. Although the data are shown up to TKE loss of 450 MeV in all figures, only points up to 400 MeV were considered in data analysis for reasons given in Sec. II. The first calculation was made with the assumption that the available excitation energy is shared according to fragment mass (dot-dashed curves) implying that thermal equilibrium is achieved during the early stages of the interaction. The second calculation was made with the assumption that the available excitation energy is shared equally (dashed curves). A third calculation (solid curves) is discussed below. In Fig. 4(b)

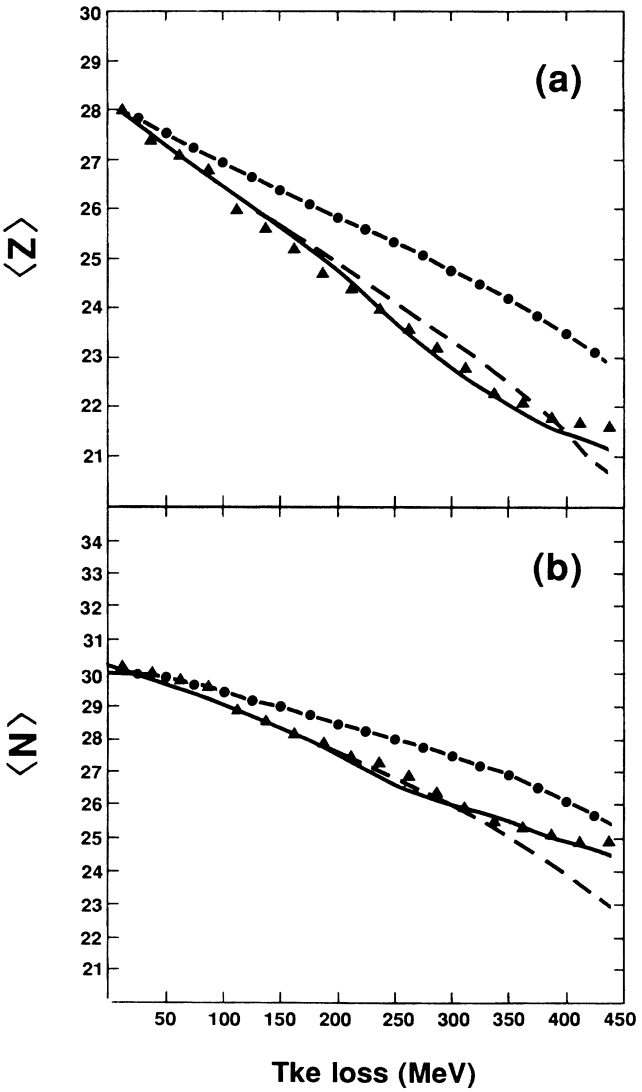

FIG. 4. Centroids of secondary (a) charge and (b) neutron distributions of PLF's. The triangles represent the data. The curves are the results of evaporation calculations using the code LILITA. Individual curves are described in the text.

the N distributions $(A-Z)$ are shown rather than mass centroids in order to determine any net neutron transfer. It is clear from the figures that the assumption of thermal equilibrium gives results which are in poor agreement with the data. The calculated centroids for charge and mass are much too large. Moreover, too little neutron emission is calculated for the PLF and too much for the TLF (Fig. 5). Except for the fair agreement between observed and calculated TLF temperatures these observations already indicate that the PLF receives a larger share of the excitation energy than its equilibrium value even for large TKE losses. On the other hand, the assumption of equal energy sharing reproduces all the observables reasonably well, except for the temperature of the TLF up to an energy loss of 325 MeV. The discrepancy between observed and calculated TLF temperature is discussed further in Sec. V.

It is surprising that, with equal energy sharing and with the charge and neutron numbers fixed at entrance channel values, such good agreement with the data is obtained. Other recent measurements[15,17,18,21-24] have indicated a transition in the sharing of available excitation energy from that of equal energy sharing to that of energy sharing according to fragment mass with increasing TKE losses. However, a closer examination of charge centroids [Fig. 4(a)] indicates that the values calculated assuming equal energy sharing are somewhat higher than the observed values in the TKE loss range of 100 MeV to 300 MeV although the N centroids [Fig. 4(b)] are in good agreement up to the TKE loss of 300 MeV. This suggests that a net transfer of charge to the target occurs at large TKE losses. Above 300 MeV TKE loss the calculated charge and N centroids fall below the observed values and the deduced TLF neutron multiplicities [Fig. 5(b)] increase rather slowly compared to the observed quantities. This suggests a transition in the sharing of the

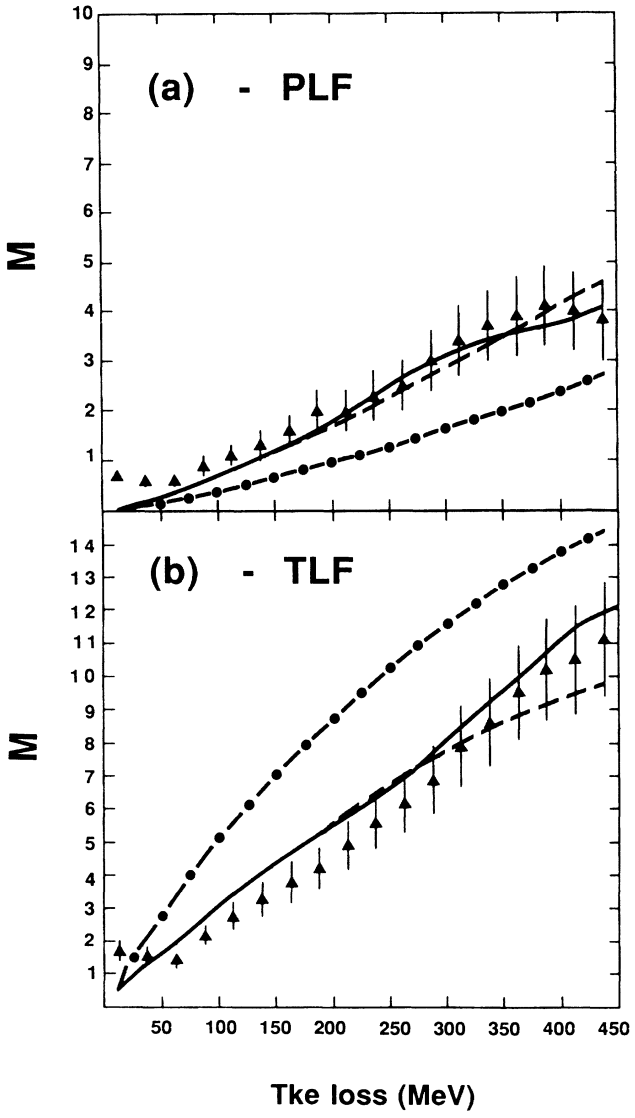

FIG. 5. Same as Fig. 4 but for multiplicities of neutrons emitted from (a) PLF and (b) TLF.

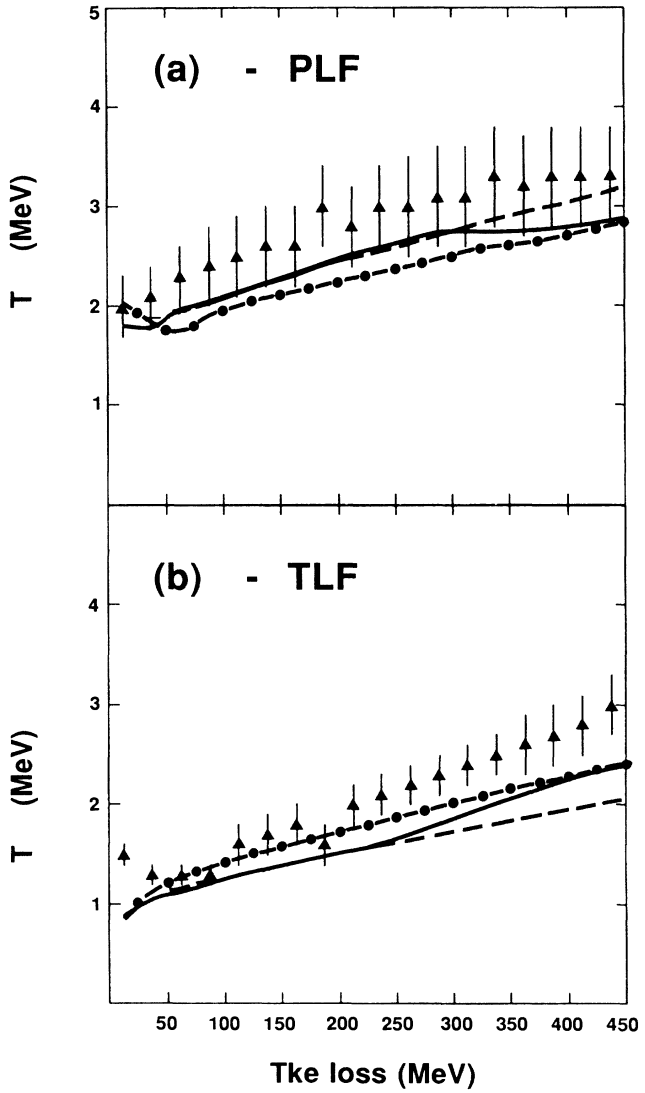

FIG. 6. Same as Fig. 4 but for the fragment temperatures deduced from the energy spectra of neutrons emitted from (a) PLF and (b) TLF.

available excitation energy from equal sharing to that of sharing in proportion to fragment mass at higher TKE losses (above 300 MeV). On the basis of these observations, combinations of primary charge centroids with net drift to the target in the TKE loss range of 100 MeV to 300 MeV and a smooth transition in excitation energy sharing from the limit of equal sharing to the limit of energy sharing in proportion to fragment masses were used as input to the evaporation code. In this analysis, at each TKE loss, three quantities (primary Z and N distribution and division of available excitation energy) were varied to reproduce six observed quantities (charge and mass centroids of PLF, and neutron multiplicities and temperatures of PLF and TLF). The results of the calculations that gave the best agreement with the data are shown as solid curves in Figs. 4–6. The average values

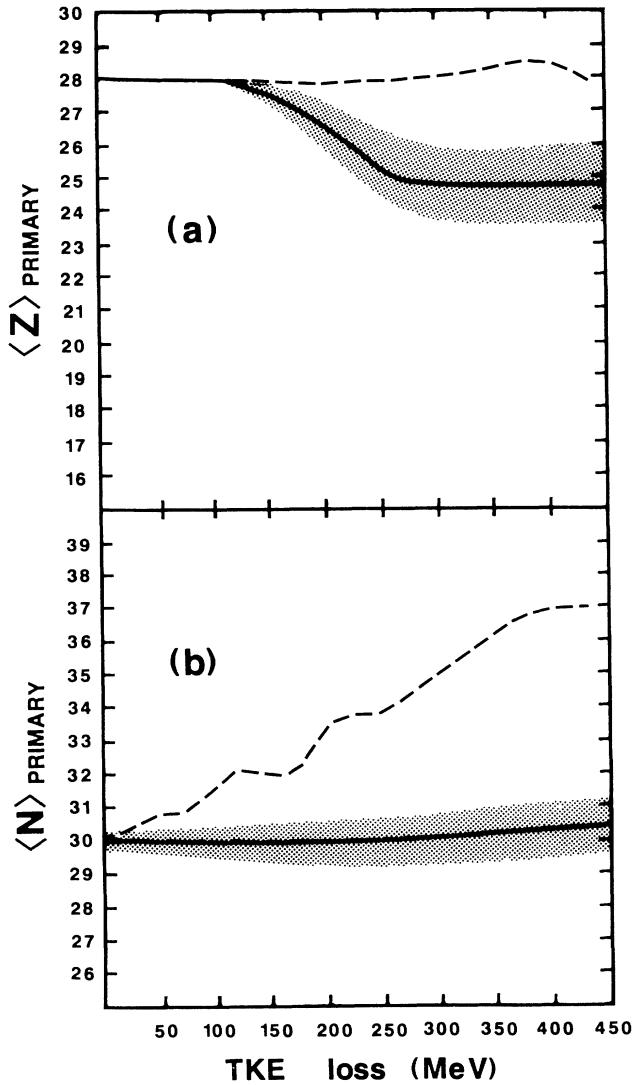

FIG. 7. Primary PLF (a) average charge and (b) average neutron number as a function of TKE loss. The solid curves represent the values deduced from evaporation calculation using experimental data. The shaded areas correspond to uncertainties in these values. The dashed curves represent the NETM predictions

TABLE II. Average primary charge and neutron number of PLF and ratio of excitation energy of the PLF relative to that of the total excitation energy deduced from calculations using the statistical model code LILITA. The results are shown as a function of TKE loss.

TKE loss (MeV)	$\langle Z \rangle$	$\langle N \rangle$	ENERGY DIVISION E^*_{PLF}/E^*_{TOTAL}
20.0	28.0±0.01	30.00±0.01	0.50±0.05
40.0	28.0±0.02	30.00±0.01	0.50±0.05
60.0	28.0±0.03	30.00±0.02	0.50±0.05
80.0	28.0±0.05	30.00±0.02	0.50±0.05
100.0	28.0±0.07	30.00±0.04	0.50±0.05
120.0	27.9±0.10	30.00±0.06	0.50±0.05
140.0	27.6±0.20	30.00±0.08	0.50±0.05
160.0	27.2±0.40	30.00±0.15	0.50±0.05
180.0	26.9±0.60	30.00±0.20	0.50±0.05
200.0	26.4±0.75	30.00±0.30	0.50±0.05
220.0	26.0±0.90	30.00±0.35	0.48±0.08
240.0	25.4±1.0	30.00±0.40	0.43±0.09
260.0	25.0±1.1	30.04±0.50	0.37±0.10
280.0	24.8±1.2	30.08±0.60	0.31±0.08
300.0	24.7±1.2	30.12±0.65	0.27±0.05
320.0	24.7±1.2	30.16±0.65	0.26±0.05
340.0	24.7±1.2	30.20±0.65	0.26±0.05
360.0	24.7±1.2	30.24±0.65	0.26±0.05
380.0	24.7±1.2	30.28±0.65	0.26±0.05
400.0	24.7±1.2	30.32±0.70	0.26±0.05
420.0	24.7±1.2	30.35±0.70	0.26±0.06

of the input primary quantities that gave the best results are tabulated in Table II and shown as solid curves in Figs. 7 and 8. The average primary charge of the PLF is shown as a function of TKE loss in Fig. 7(a) and primary neutron number in Fig. 7(b). The average primary neutron number is found to vary little from the incoming

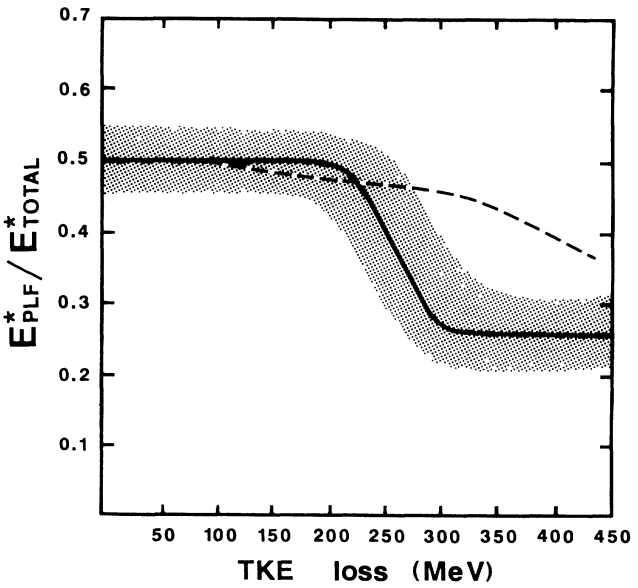

FIG. 8. Same as Fig. 7 but for E^*_{PLF}/E^*_{TOTAL}, the ratio of the excitation energy of the PLF relative to that of the total excitation energy.

projectile neutron number. The ratio of the excitation energy of the PLF relative to that of the total excitation energy is shown in Fig. 8. The shaded areas in these figures correspond to the uncertainties, which are discussed in the following section. The dashed curves in Figs. 7 and 8 are discussed in Sec. VI.

The deduced primary distributions shown in Fig. 7 indicate a net transfer of protons from PLF to TLF. On the other hand, net neutron transfer is negligible for this reaction. The N/Z ratio of the PLF gradually increases with increasing energy loss from the projectile value (1.07) and reaches a final value of 1.24, but never reaches the N/Z value (1.35) of the composite system. This behavior is in general agreement with the trends observed in other studies.[11,13,20,23,32,33] Our results are consistent with a smooth transition in available excitation energy sharing between the reaction fragments from the limit of equal energy sharing valid for TKE losses of up to approximately 200 MeV to that of energy division in proportion to the fragment masses valid at TKE losses of greater than about 300 MeV.

V. UNCERTAINTIES

The only parameter that is not represented well by the evaporation calculations is the TLF temperature. This temperature is, in fact, underpredicted by the evaporation code using almost any reasonable input data. However, in most cases, the TLF multiplicity is slightly overpredicted as illustrated by the solid curve in Fig. 5(b). Thus, the disagreement can be reduced by using a smaller value of the level density parameter for the TLF. This has the effect of increasing the predicted temperatures while decreasing the multiplicities without significantly changing any of the other parameters. A similar discrepancy between calculated and observed TLF temperatures has been reported in Refs. 18 and 24. These authors, who used a modified version of PACE instead of LILITA to perform the calculations, resorted to using a very small value $[(A/12)\ \mathrm{MeV}^{-1}]$ for the level density parameter of the TLF. In our case this does not result in completely satisfactory agreement between calculated and observed TLF temperatures over the entire range of TKE losses for any single value of the level density parameter. Since the total kinetic energy removed by neutron emission depends, in part, on the temperature, it is interesting to determine if the results of the Monte Carlo simulations correspond to a much smaller energy removal by neutron emission than the results of the moving source fits to the neutron spectra. Based on Eq. (2) the energy removed by neutron emission is given by

$$E_{\mathrm{total}} = (\tfrac{3}{2}T + S_n)M_n \qquad (3)$$

where M_n is the neutron multiplicity and S_n is the average neutron separation energy. The first term in this formula gives the energy removed in the form of neutron kinetic energy. Comparing the data points and the solid curve in Fig. 6(b) it is clear that the largest discrepancy between observed and deduced temperatures occurs at a TKE loss of approximately 250 MeV. At this point the observed and calculated temperatures differ by about 30%. However, because of the small compensating difference between calculated and observed multiplicities [Fig. 5(b)], the value of E_{total} obtained by using the observed values of M and T in Eq. (3) differ by less than 6% from the value obtained by using the calculated values. This is true for a fairly wide range of values of S_n. For S_n=7 MeV the values are 55 MeV using the observed quantities and 59 MeV using the calculated quantities. Viewed in this way, there do not appear to be any fundamental inconsistencies between the observed and calculated quantities.

The uncertainties shown as the shaded areas in Figs. 7 and 8 were estimated as described below. The uncertainties of the input quantities were estimated sequentially rather than simultaneously. To estimate the uncertainty in a particular input primary quantity, the output secondary quantity found to be most sensitive to that input was studied. Thus, for example, the uncertainty in the primary charge centroids was estimated by varying the input primary charge distribution until either the value of χ^2 evaluated between the observed and calculated secondary charge centroids was doubled or one of the neutron multiplicities (either TLF or PLF) shifted beyond the experimental uncertainties. In this procedure the other free parameters (sharing of excitation energy and primary mass distribution) were fixed at their optimum values. The temperatures were found to be very weakly correlated to the variations of primary quantities. As noted above this temperature is only a measure of the excitation energy removed in the form of neutron kinetic energy. This is a small fraction of the total excitation energy as can been seen from Eq. (3). Therefore the variations of the fragment temperatures were not used for evaluating the uncertainty in the primary quantities. In estimating the uncertainty in the sharing of excitation energy the primary charge and mass centroids used as inputs to the evaporation were fixed at their optimum values.

VI. COMPARISON WITH THE NUCLEON-EXCHANGE MODEL

It is of interest to determine whether equally satisfactory results can be obtained using specific model predictions. We have, therefore, compared our results with the nucleon-exchange transport model (NETM) of Randrup.[3] In this model the conversion of kinetic energy to internal excitation energy is accounted for by the exchange of independent nucleons between the reaction partners while they are in contact. The transport coefficients are calculated from the instantaneous conditions of the dinuclear complex in a one-body dissipation approach. This dinuclear complex is characterized by a potential of the shape of two spheres connected by a cylindrical neck. The Fokker-Planck equation is used to follow the dynamical evolution of the probability $P(N, Z; t)$

for finding Z protons and N neutrons at time t in one of the reaction fragments. These dynamical transport model calculations predict the first (centroids) and second (variance) moments for the proton and neutron number distributions and the average value for the fragment excitation energies and angular momenta.

Figures 7 and 8 show the results of this calculation compared with the results deduced as described above. In Fig. 7, the solid curve corresponds to the primary charge and neutron distributions deduced from the present experiment and the dashed curve corresponds to the NETM calculations. Figure 8 shows a similar comparison for the sharing of available excitation energy between the reaction fragments. In Fig. 7 we see significant differences between the deduced primary charge and neutron distributions and the primary distributions obtained from the NETM. The model calculations predict almost no net proton transfer and a large net transfer of neutrons to the PLF in the TKE loss region considered here which indicates a drift towards mass symmetry. In the model calculations, the N/Z ratio for higher TKE losses reaches N/Z value (1.35) of the dinuclear composite system. In contrast, the experimental data show a net transfer of protons to the TLF with negligible net neutron drift. This discrepancy is very similar to the observations reported in Ref. 23. Also the model predicts a much more gradual transition (Fig. 8) in the sharing of available excitation energy from the limit of equal energy sharing to the limit of energy sharing in proportion to fragment masses than the experimentally deduced transition.

The predictions for the measured secondary quantities from the evaporation code LILITA, with input primary charge and mass distributions and fragment excitation energy and angular momenta as predicted from the NETM are compared with data in Figs. 9–11. It is clearly

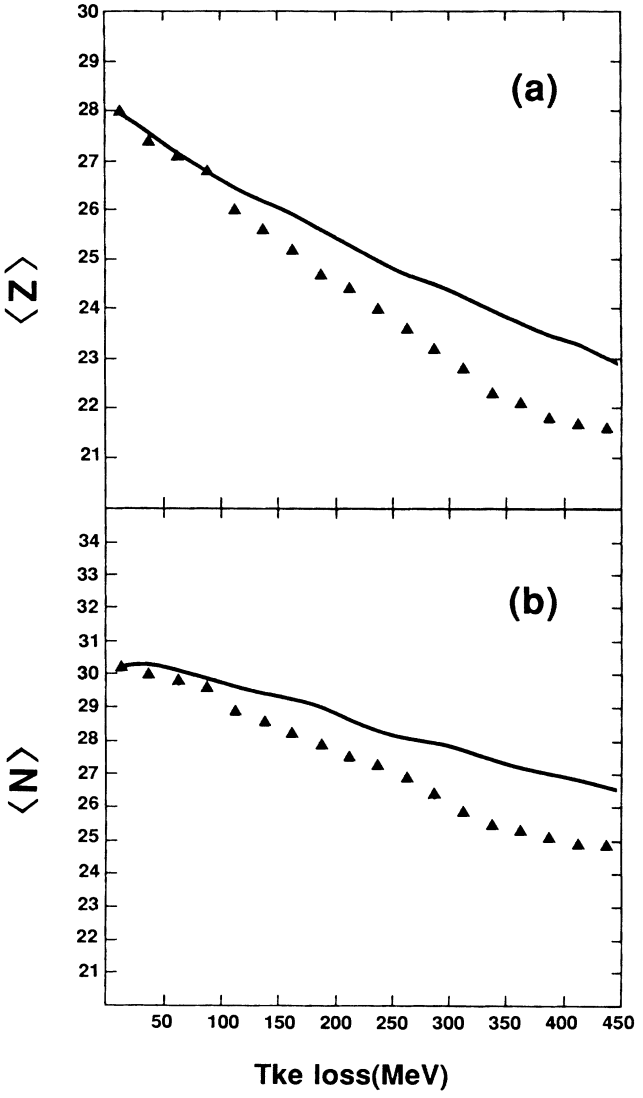

FIG. 9. Comparison of measured PLF secondary (a) charge and (b) neutron centroids with statistical evaporation calculations using the nucleon exchange model predictions for the primary fragment distributions. The triangles represent the data. The solid curves indicate the calculated results.

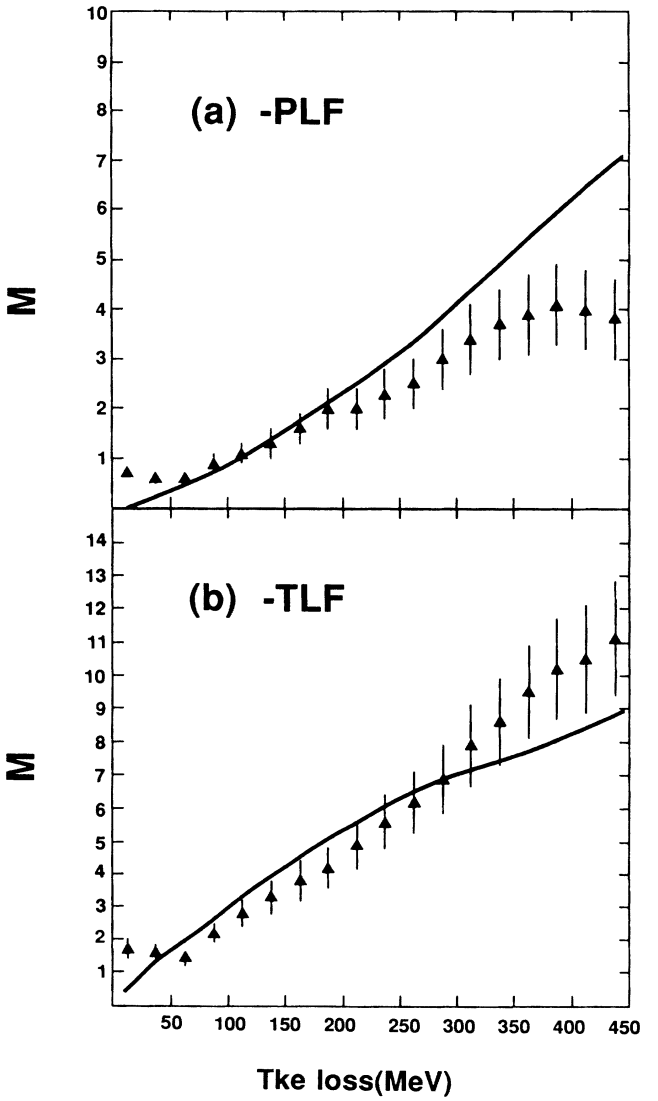

FIG. 10. Same as Fig. 9 but for multiplicities of neutrons emitted from (a) PLF and (b) TLF.

seen from these figures that the statistical evaporation model calculation with input from the nucleon exchange model predictions is in poor agreement with the data. The calculated secondary centroids for charge and neutron numbers overestimate the data at higher TKE losses (above 100 MeV). The calculated PLF multiplicities increase more steeply and the TLF multiplicities increase more gradually than the measured values for higher TKE losses (250 MeV) but the temperature extracted from the spectra of neutrons emitted from PLF and TLF predicted by this calculation agree with data equally as well as temperatures predicted by the evaporation code using the deduced primary distributions. This again indicates the weak correlation between the extracted temperatures and the input primary distributions.

The second moments σ_Z^2 and σ_N^2 of the secondary charge and neutron number distributions are shown in Fig. 12. The experimental results (triangles) are compared with the predictions of the statistical model calculations with the results of the NETM used as input to the evaporation code as described above (solid curves). The widths of the experimental distributions are significantly larger than the predicted widths at large values of the TKE loss. This discrepancy may be attributed to the neglect of two-body collisions in the NETM which would be expected to broaden the primary distribution.[34]

VII. SUMMARY

We have measured secondary charge and mass distributions of PLF, neutron multiplicities and temperatures of PLF and TLF for strongly damped reactions of ^{58}Ni+^{165}Ho at 16 MeV/nucleon. These measurements together with the statistical evaporation code LILITA

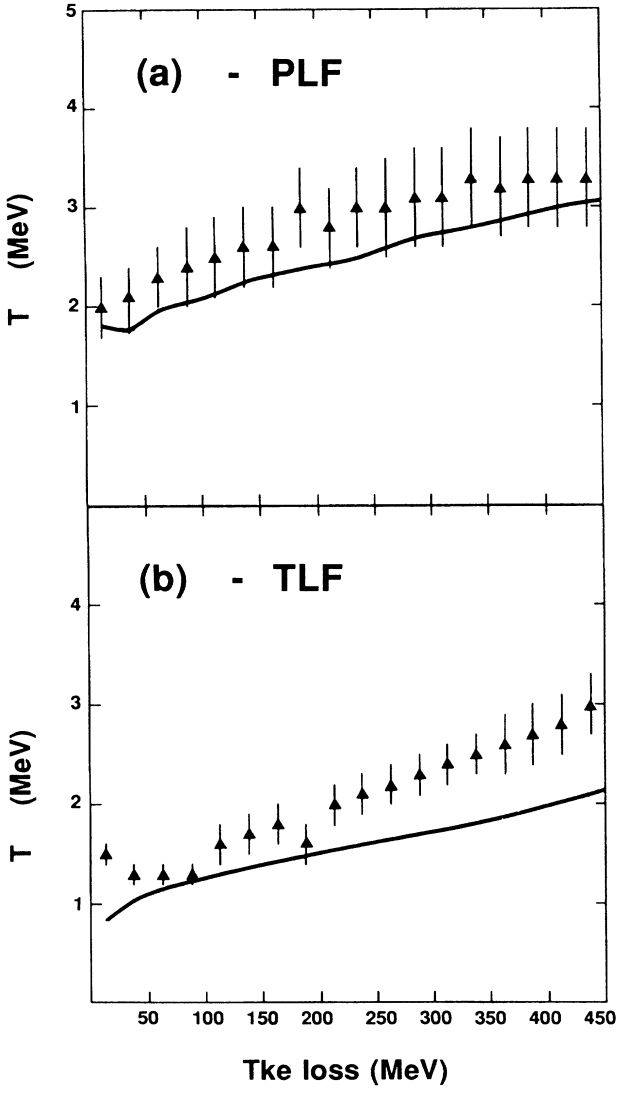

FIG. 11. Same as Fig. 9 but for the fragment temperatures deduced from the energy spectra of neutrons emitted from (a) PLF and (b) TLF.

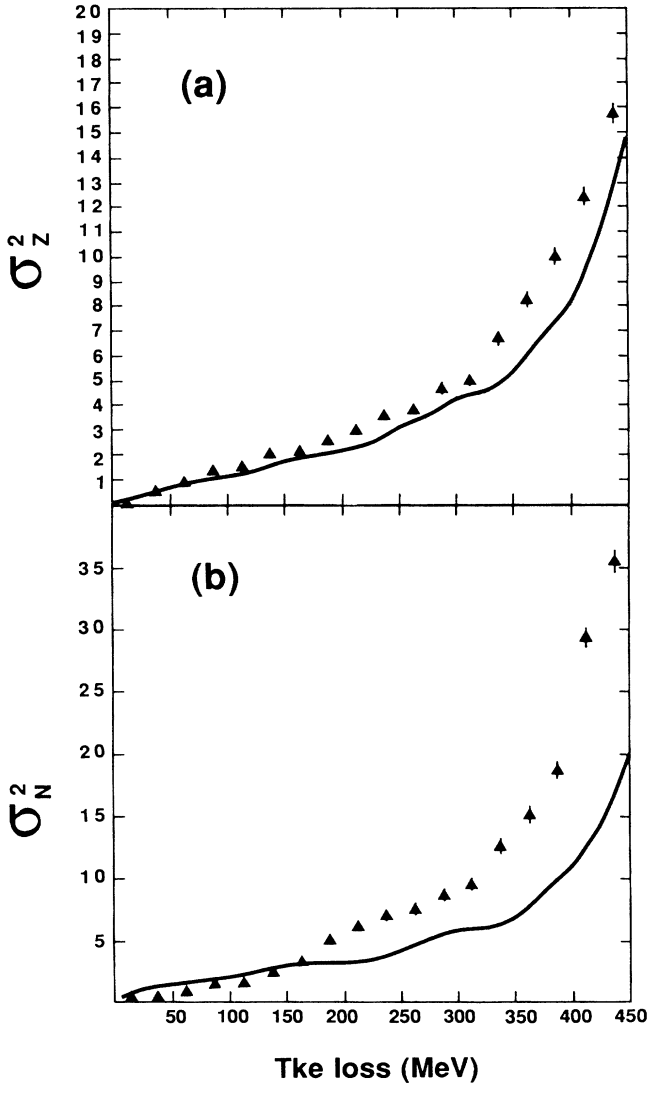

FIG. 12. Comparison of measured (a) charge and (b) neutron variances with nucleon exchange model predicted variances. The solid curves correspond to the model predictions.

were used to deduce the primary charge and mass centroids and the division of the available excitation energy between the reaction partners as a function of the TKE loss. The deduced primary centroids indicate a net transfer of protons from PLF to TLF and no net neutron drift with increasing TKE loss. This conclusion is in contradiction to predictions of the nucleon exchange model.[3] The data also indicate a more rapid transition than predicted by the model from equal excitation energy division to thermal energy division.

The experimental secondary PLF neutron and proton number distribution variances are observed to be larger than predicted by the nucleon exchange transport model.

ACKNOWLEDGMENTS

The authors wish to thank J. Randrup for providing us with the transport model calculations. This work is supported by the U.S. Department of Energy, under Contract Nos. DE-FG05-84ER40162 with Georgia State University and DE-AC05-84OR21400 with Martin Marietta Energy Systems.

[1] W. U.Schröder and J. R. Huizenga, in *Treatise on Heavy-Ion Science*, edited by D.A. Bromley (Plenum, New York, 1984).

[2] W. Nörenberg, Phys. Lett. **B53**, 289 (1974).

[3] J. Randrup, Nucl. Phys. **A307**, 319 (1978); **A327**, 490 (1979); **A383**, 468 (1982); T. Dossing, and J. Randrup, *ibid.* **A433**, 280 (1985); J. Randrup and R. Vandenbosch, *ibid.* **A474**, 219 (1987).

[4] S. K. Samaddar, J. N. De, and K. Krishan, Phys. Rev. C **31**, 1053 (1985).

[5] D. K. Lock, R. Vandenbosch, and J. Randrup, Phys. Rev. C **31**, 1268 (1985).

[6] Y. Eyal, A. Gavron, I. Tserruya, Z. Fraenkel, Y. Eisen, S. Wald, R. Bass, C. R. Gould, G. Kreyling, R. Renfordt, K. Stelzer, R. Zitsmann, A. Gobbi, U. Lymen, H. Stelzer, I. Rode, and R. Bock, Phys. Rev. Lett. **41**, 625 (1978).

[7] B. Tamain, K. Chechik, H. Fuchs, F. Hanappe, M. Morjian, C. Ngô, J. Peter, M. Dakowski, B. Lucas, C. Mazur, M. Ribrag, and C. Signarbieux, Nucl. Phys. **A330**, 253 (1979); J. Peter, M. Berlanger, C. Ngô, B. Tamain, B. Lucas, C. Mazur, M. Ribrag, and C. Signarbieux, Z. Phys. A **283**, 413 (1977).

[8] B. Cauvin, R. C. Jared, P. Russo, R. P. Schmidtt, R. Babinet, and L. Moretto, Nucl. Phys. **A301**, 511 (1978); R. Babinet, B. Cauvin, J. Girard, H. Nifenecker, B. Gatty, D. Guerreau, M. Lefort, and X. Tarrago, *ibid.* **A296**, 160 (1978).

[9] D. Hilscher, J. R. Birkelund, A. D. Hoover, W. U. Schröder, W. W.Wilcke, J. R. Huizenga, A. C. Mignerey, K. L. Wolf, H. F. Breuer, and V. E. Viola, Phys. Rev. C **20**, 576 (1979).

[10] H. Breuer, B. G. Glagola, V. E. Viola, K. L. Wolf, A. C. Mignerey, J. R. Birkelund, D. Hilscher, A. D. Hoover, J. R. Huizenga, W. U. Schröder, and W. W. Wilcke, Phys. Rev. Lett. **43**, 191 (1979).

[11] H. C. Britt, B. H. Erkkila, A. Gavron, Y. Patin, R. H. Stokes, M. P. Webb, P. R. Christensen, O. Hansen, S. Pontoppidan, F. Vidabeck, R. L. Ferguson, F. Plasil, G. R. Young, and J. Randrup, Phys. Rev. C **26**, 1999 (1982).

[12] I. Tserruya, A. Breskin, R. Chechik, Z. Fraenkel, S. Wald, N. Zwang, R. Bock, M. Dakowski, A. Gobbi, H. Sann, R. Bass, G. Kreyling, R. Renfordt, K. Stelzer, and U. Arlt, Phys. Rev. C **26**, 2509 (1982).

[13] H. Breuer, A. C. Mignerey, V. E. Viola, K. L. Wolf, J. R. Birkelund, D. Hilscher, J. R. Huizenga, W. U. Schröder, and W. W. Wilcke, Phys. Rev. C **28**, 1080 (1983).

[14] H. R. Schmidt, S. B. Gazes, Y. Chan, R. Kamermans, and R. G. Stokstad, Phys. Lett. B **180**, 9 (1986).

[15] T. C. Awes, R. L. Ferguson, R. Novotny, F. E. Obenshain, F. Plasil, S. Pontoppidan, V. Rauch, G. R. Young, and H. Sann, Phys. Rev. Lett. **52**, 251 (1984).

[16] R. Vandenbosch, A. Lazzarini, D. Leach, D. K. Lock, A. Ray, and A. Seamster, Phys. Rev. Lett. **52**, 1964 (1984).

[17] D. R. Denton, H. Breuer, F. Khazaie, K. Kwiatkowski, V. E. Viola, S. Bradley, A. C. Mignerey, and A. P. Weston-Dawkes, Phys. Rev. C **38**, 1207 (1988); D. R. Denton, H. Breuer, F. Khazaie, K. Kwiatkowski, V. E. Viola, S. Bradley, A. C. Mignerey, A. P. Weston-Dawkes, and R. J. McDonald, Phys. Lett. B **185**, 326 (1987).

[18] J. L. Wile, W. U. Schröder, J. R. Huizenga, and D. Hilscher, Phy. Rev. C **35**, 1608 (1987).

[19] L. G. Sobotka, G. T. Wozniak, R. J. McDonald, M. A. McMahan, R. J. Charity. L. G. Moretto, Z. H. Lui, F. S. Stephens, R. M. Diamond, M. A. Deleplanque, and A. J. Pacheco, Phys. Lett. B **175**, 27 (1986).

[20] R. T. de Souza, W. U. Schröder, J. R. Huizenga, R. Płaneta, S. H. Zhou, V. E. Viola, and H. Breuer, Phys. Rev. C **37**, 1783 (1988).

[21] R. Płaneta, S. H. Zhou, K. Kwiatkowski, W. G. Wilson, and V. E. Viola, Phys. Rev. C **38**, 195 (1988).

[22] R. Płaneta, K. Kwiatkowski, S. H. Zhou, V. E. Viola, H. Breuer, M. A. McMahan, J. Randrup, and A. C. Mignerey, Phys. Rev. C **39**, 1197 (1989).

[23] R. Płaneta, K. Kwiatkowski, S. H. Zhou, V. E. Viola, H. Breuer, M. A. McMahan, W. Kehoe and A. C. Mignerey, Phys. Rev. C **41**, 942 (1990).

[24] J. L. Wile, S. S. Datta, W. U. Schröder, J. R. Huizenga, R. T. de Souza and D. Pade, Phys. Rev. C **40**, 1700 (1989).

[25] H. Sohlbach, H. Freiesleben, P. Braun-Munzinger, W. F. W. Schneider, D. Schüll, B. Kohlmeyer, M. Marinescu, and F. Puhlhofer, Phys. Lett. **153B**, 386 (1985); Nucl. Phys. **A467**, 349 (1987).

[26] R. Dayras, R. Coniglione, J. Barrette, B. Berthier, D. M. de Castro Rizzo, O. Cisse, F. Gadi, R. Legrain, M. C. Mermaz, H. Delagrange, W. Mittig, B. Heusch, G. Lanzano, and A. Pagano, Phys. Rev. Lett. **62**, 1017 (1989).

[27] M. Korolija, N. Cindro, and R. Caplar, Phys. Rev. Lett. **60**, 193 (1988).

[28] G. A. Petitt, C. Butler, V. Penumetcha, T. C. Awes, J. R. Beene, F. E. Obenshain, F. Plasil, S. P. Sorensen, and G. R. Young, Phys. Rev. C **40**, 692 (1989).

[29] Program LILITA, J. Gomez del Campo and R. G. Stokstad, Oak Ridge National Laboratory. Modified by S. P.

Sorensen, University of Tennessee (unpublished).
[30]A. Gavron, Phys. Rev. C **21**, 230 (1980).
[31]L. G. Moretto, in *Nuclear Structure and Heavy-Ion Collisions*, Proceedings of the International School of Physics "Enrico Fermi," Course LXXVII, Varenna, Italy, 1979, edited by R. A. Broglia, R. A. Ricci, and C. H. Dasso (North-Holland, New York, 1981).
[32]H. Freiesleben and J. V. Kratz, Phys. Rep. **106**, 1 (1984).
[33]K.E. Rehm, A. M. Van de Berg, J. J. Kolata, D. G. Kovar, W. Kutschera, G. Rosner, G. S. F. Stephans, and J. L. Yntema, Phys. Rev. C **37**, 2629 (1988).
[34]S. Ayik, Phys. Rev. C **35**, 2086 (1987).

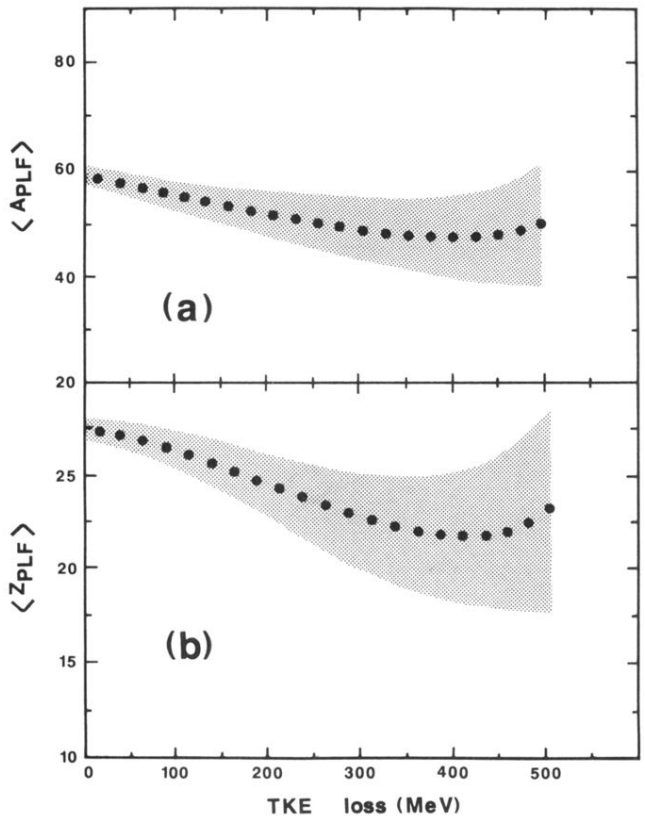

FIG. 3. Centroids of secondary PLF distributions in (a) charge and (b) mass as a function of TKE loss, determined from a moment analysis. The shaded areas surrounding the data points extend to one standard deviation from the average values.

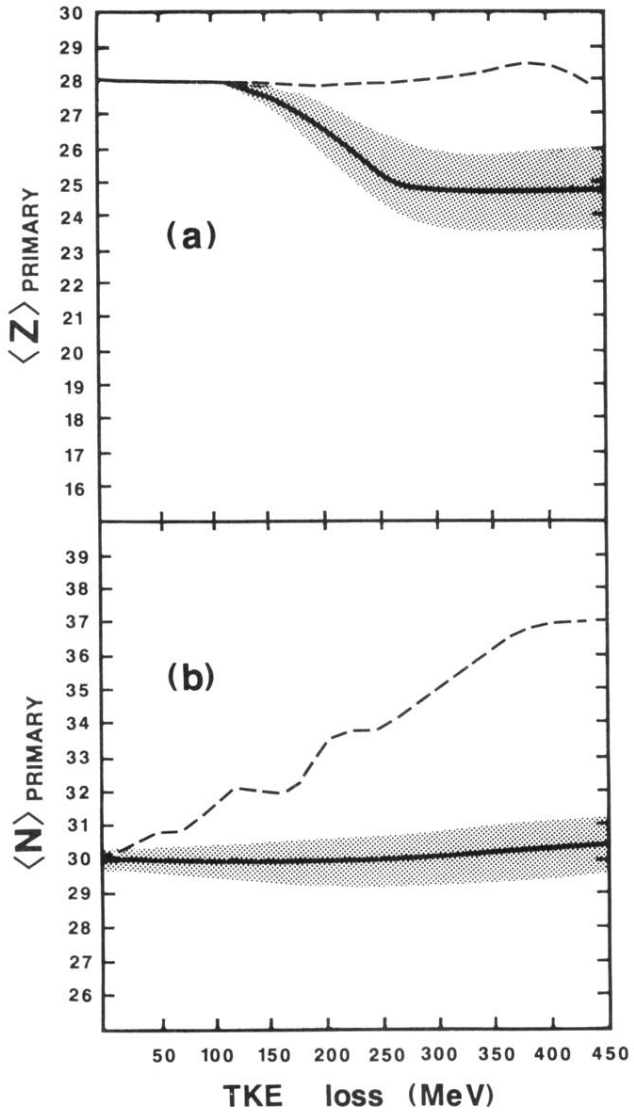

FIG. 7. Primary PLF (a) average charge and (b) average neutron number as a function of TKE loss. The solid curves represent the values deduced from evaporation calculation using experimental data. The shaded areas correspond to uncertainties in these values. The dashed curves represent the NETM predictions

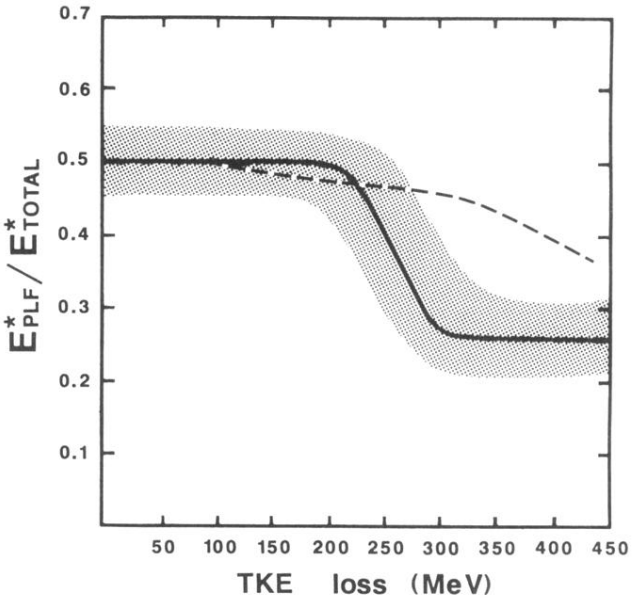

FIG. 8. Same as Fig. 7 but for $E^*_{\mathrm{PLF}}/E^*_{\mathrm{TOTAL}}$, the ratio of the excitation energy of the PLF relative to that of the total excitation energy.